nature physics

Article

https://doi.org/10.1038/s41567-024-02540-x

Active hydraulics and odd elasticity of muscle fibres

Received: 24 October 2022

Accepted: 6 May 2024

Published online: 08 July 2024

Check for updates

Suraj Shankar [1,2] & L. Mahadevan [1,3,4]

Muscle is a complex, hierarchically organized, soft contractile engine. To understand the limits on the rate of contraction and muscle energetics, we construct a coarse-grained multiscale model that describes muscle as an active sponge. Our analysis of existing experiments across species and muscle types highlights the importance of spatially heterogeneous strains and local volumetric deformations. Our minimal theoretical model shows how contractions induce intracellular fluid flow and power active hydraulic oscillations, yielding the limits of ultrafast muscular contractions. We further demonstrate that the viscoelastic response of muscle is naturally non-reciprocal—or odd—owing to its active and anisotropic nature. This enables an alternate mode of muscular power generation from periodic cycles in spatial strain alone, contrasting with previous descriptions based on temporal cycles. Our work suggests a revised view of muscle dynamics that emphasizes the multiscale spatiotemporal origins of soft hydraulic power, with potential implications for physiology, biomechanics and locomotion.

Muscle is the primary driver of nearly all motion across the animal kingdom. Since the pioneering work by H. E. Huxley, A. F. Huxley and others[1,2], much work has focused on the molecular aspects of the contractile machinery, for example, actomyosin motor kinetics[3–5] and calcium signalling[6]. But muscle fibres are spatially and hierarchically organized across multiple scales[7] (Fig. 1a) with complex structural and mechanical properties: striated muscle fibres are soft, wet and active materials composed of a dense, anisotropic and actively contracting polymeric lattice (sarcomeres forming the myofibril), bathed in cytosol. Water, although the dominant component of muscle fibres (70–90% by volume[7,8]), is assumed to play a passive role, subservient to biochemical processes. In recent years, however, intracellular fluid flows have increasingly been recognized for their central role in dictating cellular morphology, motility and physiology[9,10]—for example, in rapid non-muscular movements in plants[11].

As muscle can operate at frequencies ranging between 10^2 and 10^3 Hz (refs. 12,13), with power outputs of ~5–500 W kg^{-1} (ref. 14), it naturally raises questions about the biophysical mechanisms underlying the dynamical limits of performance. Given the large fraction of water in muscle, here we investigate the potential role of spatial hydraulic effects in the dynamics of contracting muscle fibres. In Fig. 1b we show a coarse-grained view that suggests how muscle fibres behave as an active fluid-filled sponge. When a muscle fibre contracts, there must be relative and spatially inhomogeneous movement of the actomyosin filament lattice relative to the ambient fluid (due to global incompressibility in the presence of an intact sarcolemma). Local deformations must squeeze fluid through the pores of the myofilament lattice, although the dynamical consequences of this process are typically neglected as most in vitro studies focus on glycerinated (permeabilized) muscle fibres that allow free drainage of fluid[8].

Early experiments by Szent-Györgi[15,16] on extracted actomyosin threads highlighted the syneresis associated with expelling water as they 'violently contract' (Fig. 1c), and other studies have noted water movements in muscle due to osmolytes, contractions and so on[17,18]. Since then, molecular studies have shown that active crossbridges produce both longitudinal and transverse (radial) strains; the latter lead to sarcomere volume change[19] and fluid redistribution. Spatially non-uniform strains (Fig. 1d) have also been associated with intact muscle fibre contractions ex vivo[20,21] and in vivo[22], suggesting that the concomittant pressure and hydraulic flows may all be relevant

[1]Department of Physics, Harvard University, Cambridge, MA, USA. [2]Department of Physics, University of Michigan, Ann Arbor, MI, USA. [3]Paulson School of Engineering and Applied Sciences, Harvard University, Cambridge, MA, USA. [4]Department of Organismic and Evolutionary Biology, Harvard University, Cambridge, MA, USA. e-mail: surajsh@umich.edu; lmahadev@g.harvard.edu

https://doi.org/10.1038/s41567-024-02540-x

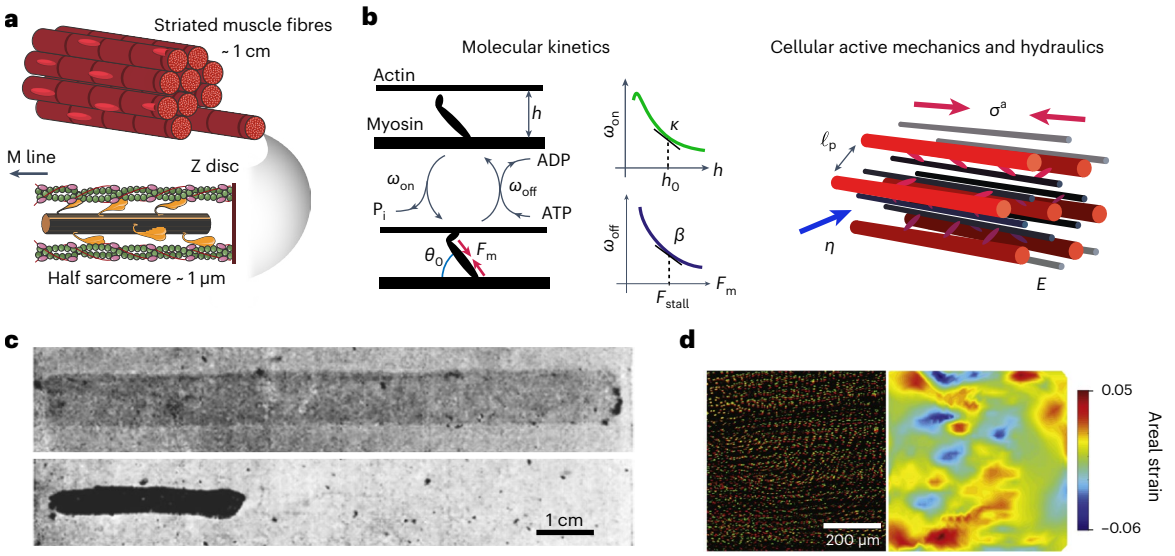

Fig. 1 | Muscle fibres are multiscale soft, wet, active engines. a, Striated muscle consists of long, multinucleated fibres that span several spatial scales, ranging from the contractile machinery in periodically repeating sarcomeres (~1 μm) to macroscopic fibres that can span 1–10 cm. **b**, A multiscale mathematical model of muscle fibres (equations (1)–(5)). On the molecular scale (left), stochastic binding of myosin motor heads to actin generates a contractile force (F_m) upon hydrolysing ATP, with both radial and axial components for a finite crossbridge binding angle (θ_0). Kinetic rates ($\omega_{on/off}$) decrease with increasing interfilament spacing (h) and F_m, with κ and $\beta > 0$ measuring the linearized feedback at rest and under stall conditions, respectively (see Supplementary Section I for details). On the mesoscale (right), the myofilament lattice is an anisotropic elastic network with an elastic modulus E and pore size ℓ_p that is permeated by a fluid of viscosity η and contracts due active stresses (σ^a). **c**, Actomyosin threads contract by expelling water, changing both shape and size when placed in boiled muscle juice, a source of ATP. **d**, In vivo contraction of an electrically stimulated skeletal muscle (murine gastrocnemius) displaying spatial strain heterogeneities (right: heatmap of the 2D areal strain) measured using the stained nuclei as fiducial markers (green, undeformed; red, deformed). Panels adapted with permission from: **c**, ref. 16, Springer Nature; **d**, ref. 22, Elsevier. Panel **a** created using Servier Medical Art images (muscle fibre and actin) from Bioicons.

dynamically. Recent optical and X-ray scattering experiments probing the rapid dynamics of the myofilament lattice[23–28] further quantify these observations.

A reanalysis of data on active oscillations of muscle fibres from experiments on different muscle types and species allowed us to obtain time traces of local transverse ($\epsilon_\perp$) and longitudinal (ϵ_{zz}) strains in the sarcomere (Fig. 2; see Supplementary Section VA for details). As an example, in Fig. 2a,b we show that the contractile oscillations with frequency $\omega \approx 1$ Hz in glycerinated skeletal muscle fibres (rabbit psoas[23,24]) lead to strains that are not volume preserving; that is, they are non-isochoric (Fig. 2, black line) despite the fibres being permeabilized. This is probably because the fibres are slender enough to lack radial gradients in deformation (Supplementary Section IIIB). In vivo measurements of the sarcomere geometry in intact asynchronous flight muscle of *Drosophila*[25,26] show that the lattice contracts with a constant lattice spacing[26], hence $\epsilon_\perp \approx 0$ under natural flight conditions (wing-beat frequency $\omega \approx 156$ Hz; Fig. 2c). Intact synchronous flight muscle of *Manduca sexta* also displays periodic lattice dilations and contractions under physiological conditions ($\omega \approx 25$ Hz; Fig. 2d), both in vivo[28] and ex vivo[27]. In all of the above examples (with and without a membrane), the deforming myofilament lattice fails to preserve its local volume ($\epsilon_{zz} + \epsilon_\perp \neq 0$), implying that there must be fluid movement through the sarcomere consistent with spatiotemporal strain heterogeneities.

In light of the evidence summarized above, we need to build a model that captures and explains the three-dimensional (3D) and volumetric deformations in muscle fibres. Current approaches employ detailed, spatially explicit computational models of muscle contraction (see refs. 7,29 and references therein) and have begun to include the role of fluid flow[27,30,31], but largely ignore the multiscale, elastic, active and spatial aspects of the problem. Here we adopt a complementary perspective by developing a minimal continuum model that identifies the relevant coarse-grained variables and key dimensionless parameters, and highlights general biophysical principles about cellular constraints on muscular performance limits.

We do this by adapting the theory of poroelasticity, which describes fluid-filled porous elastic materials[32]. In Fig. 1b we present our generalization of this framework that integrates molecular actomyosin kinetics with anisotropic elasticity, activity and flow to describe muscle fibres as a self-squeezing sponge.

Biophysical model

We model the muscle fibre as a cylinder (length L, radius R) lying along the $\hat{z}$ axis, made of a biphasic mixture of an active porous solid (ϕ: solid fraction) immersed in fluid ($1-\phi$: fluid fraction). The interdigitated arrangement of filaments and flexible proteins endows the sarcomere with a uniaxially anisotropic elastic stress (σ^{el}) that is linearly related to the strain tensor $\epsilon = [\nabla\mathbf{u} + (\nabla\mathbf{u})^T]/2$ (displacement $\mathbf{u} = u_r\hat{\mathbf{r}} + u_z\hat{\mathbf{z}}$, with radial u_r and axial u_z components, assuming axisymmetry), where the drained elastic moduli are functions of ϕ (see Supplementary Section IA for details). The passive elastic response of the porous solid is both anisotropic and compressible, approaching the incompressible limit only as $\phi \to 1$. In addition to the passive stress, molecular interactions between the thick (myosin) and thin (actin) filaments lead to an active stress (σ^a). The fluid stress in the composite is dominated on large scales by an isotropic pressure p, whose gradients drive a flow velocity (v) with viscous dissipation being consequential only on the scale of the hydraulic pore size $\ell_p \approx 20$–55 nm (refs. 7,8) (see Supplementary Section IA for details). We emphasize that viscous forces are important on small scales, not because they balance individual motor forces (they do not[1,31]), but because they balance large-scale spatial gradients ($\sim 1/L$) of the active stress. Mass and momentum conservation then collectively dictate overall force balance, global incompressibility and force balance in the fluid as follows (see Supplementary Section IA for details):

$$\nabla \cdot [\phi(\sigma^a + \sigma^{el}) - (1-\phi)p1] = \mathbf{0}\,, \qquad (1)$$

https://doi.org/10.1038/s41567-024-02540-x

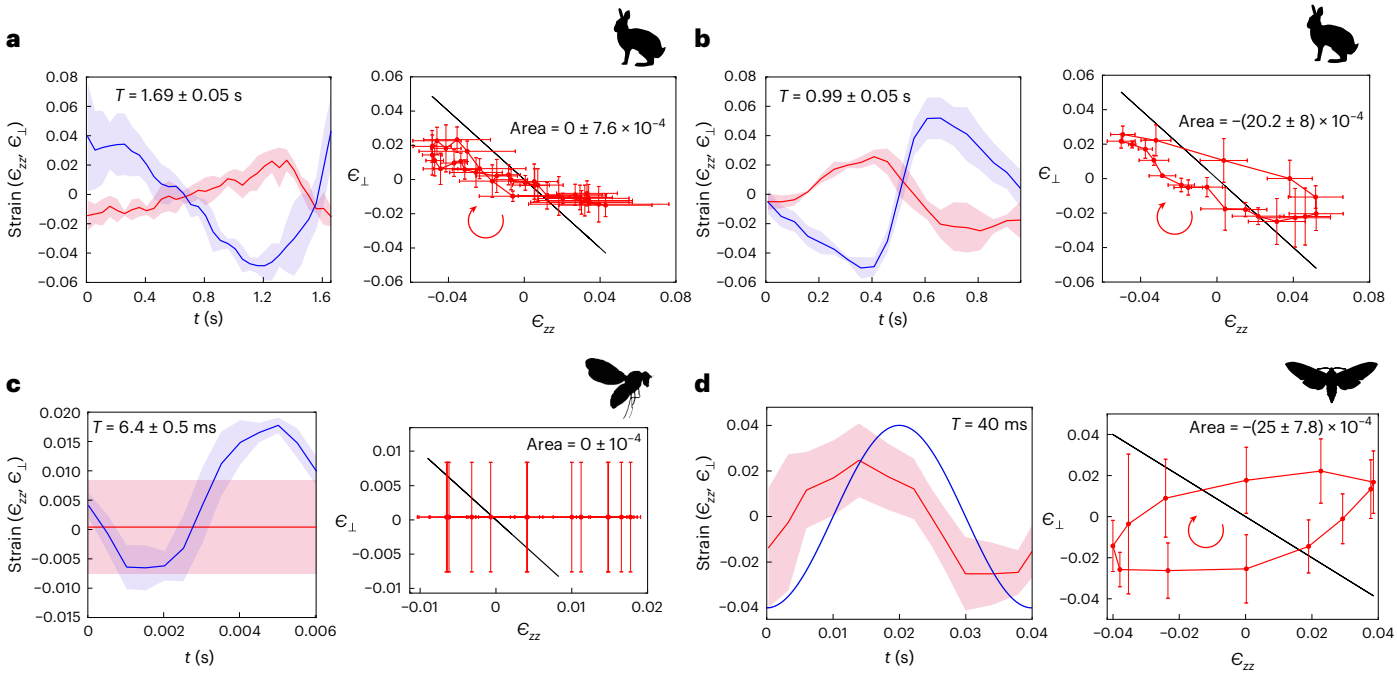

Fig. 2 | Volume changes and strain cycles are generic in self-oscillating muscle. Left, volume changes, with time period T. Right, strain cycles. **a**,**b**, Skinned rabbit psoas muscle fibres exhibit spontaneous sarcomeric oscillations in vitro under different ATP concentrations and sarcomere resting lengths[23,24]: at low ATP concentrations (**a**) ϵ_{zz} (blue) and $\epsilon_\perp$ (red) oscillate nearly antiphase with frequency $\omega \approx 0.6$ Hz (ref. 24), whereas at higher ATP concentrations (**b**), faster oscillations ($\omega \approx 1$ Hz) develop a strain cycle[23] that encloses a significant (signed) area (see Supplementary Section VA). The direction of cycling is shown by the red arrow. **c**, In vivo measurements of strain in asynchronous flight muscle (DLM, dorsal longitudinal) of a fruit fly in tethered flight ($\omega \approx 156$ Hz)[25,26] (see Supplementary Section VA for details) from time-resolved optical and X-ray measurements showing negligible $\epsilon_\perp \approx 0$. **d**, Ex vivo measurements of strain in intact synchronous flight muscle (DLM) from *M. sexta* (hawkmoth)[27], displaying non-isochoric strain cycles. The isolated, whole muscle is subject to oscillatory stretch (4% axial strain, $\omega = 25$Hz) and electrical stimulation (activation phase of 0.5), matching physiological in vivo conditions. Deformations in **a**–**d** are generically not isochoric ($\epsilon_{zz} + \epsilon_\perp = 0$, black line) and as a result fluid flow is inevitable. The data are presented as mean with shaded regions and error bars in **a**–**c** denoting 1 s.d. from averaging over multiple periods and error bars in **d** the 95% confidence intervals (sample size is 1 in all). See Supplementary Section VA for further details of the analysis. Credit: animal silhouettes, PhyloPic.

$$\nabla \cdot [\phi \partial_t \mathbf{u} + (1-\phi)\mathbf{v}] = \mathbf{0}\,, \tag{2}$$

$$(1-\phi)(\mathbf{v} - \partial_t \mathbf{u}) = -\frac{\ell_p^2}{\eta} K \cdot \nabla p\,, \tag{3}$$

where η is the fluid viscosity and $K(\phi) = K_\parallel(\phi)\hat{\mathbf{z}}\hat{\mathbf{z}} + K_\perp(\phi)(1 - \hat{\mathbf{z}}\hat{\mathbf{z}})$ is a ϕ-dependent anisotropic permeability tensor (see Supplementary Section IA for details). We note that the anisotropic structure of the sarcomere ensures that the lattice becomes radially impermeable to fluid flow ($K_\perp \to 0$ when $\phi \approx 0.91$, see Supplementary Section IA for details) before becoming incompressible ($\phi \to 1$). Hence volumetric deformations leading to intracellular flow are inevitable for all physiologically relevant $\phi \approx 0.1$–0.22 (refs. 7,8).

To complete the formulation of the problem, we need to determine the active stress σ^a that depends on the action of the actomyosin engine. In terms of a simple two state model where $n_m(x,t)$ is the coarse-grained fraction of bound myosin motors and $\langle y \rangle(x,t)$ is the average extension of the motor head at a given time t and position x in the cell, the coupled dynamics of the actomyosin crossbridges is then given by (see Supplementary Section IB for details):

$$\partial_t n_m = \omega_{on}(\epsilon_\perp)(1 - n_m) - \omega_{off}(\langle y \rangle) n_m\,, \tag{4}$$

$$\partial_t \langle y \rangle = y_0 \left(\lambda_\parallel \partial_t \epsilon_{zz} + \lambda_\perp \partial_t \epsilon_\perp\right) - \omega_{on}(\epsilon_\perp)\left(\frac{1 - n_m}{n_m}\right)(\langle y \rangle - y_0)\,, \tag{5}$$

where $y_0 \simeq 8$–10 nm (ref. 1) is the motor displacement generated during the power stroke and $\lambda_\parallel$ and $\lambda_\perp$ are factors associated with the geometry of the binding crossbridge[33,34] (see Supplementary Section IB for details). In Fig. 1b (see Supplementary Section IB for details) we show how to account for feedback through the known load-dependent unbinding rate ($\omega_{off}(\langle y \rangle)$) (ref. 35) via stretch activation[36] and a strain- or lattice-spacing-dependent binding rate ($\omega_{on}(\epsilon_\perp)$) (refs. 8,33,37) that allow the length-based regulation of force underlying the well-known Frank–Starling law[2]. As $\omega_{on/off}$ represent effective coarse-grained kinetic rates, we did not distinguish between different microscopic mechanisms of feedback. Assuming that the myosin head behaves like a spring with stiffness k_m, size d_m and a linear density N along the thick filament, the active contractile force density is $F_m = -k_m n_m \langle y \rangle$, which gives rise to an anisotropic active stress $\sigma^a = -N d_m F_m\,[\,\cos^2\theta_0 \hat{\mathbf{z}}\hat{\mathbf{z}} + (\sin^2\theta_0/2)(1 - \hat{\mathbf{z}}\hat{\mathbf{z}})]$. The active stress importantly includes both axial and radial components of the active force, which are governed by the average crossbridge binding angle θ_0 (refs. 33,34) (Fig. 1b; see Supplementary Section IB for details). Equations (1)–(5), supplemented by appropriate boundary and initial conditions, complete the specification of our multiscale continuum model.

Active hydraulic oscillations

To understand the dynamical consequences of the model, we consider two simple limits. In the passive, isotropic limit ($\sigma^a = 0$, $K_\parallel = K_\perp$), we recover the classical result[32] that p equilibrates diffusively over L on a poroelastic timescale $\tau_p \approx (\eta/E)(L/\ell_p)^2$ (see Supplementary Section II for details), that combines the rheological (η, E) with the microstructural (ℓ_p). Anisotropy generalizes this result by distinguishing axial from radial flow.

In contrast, in the active case, upon neglecting spatial heterogeneities and fluid flow ($\nabla p \simeq 0$), our model matches previous kinetic theories of molecular motor assemblies[38], where the kinetic timescale

https://doi.org/10.1038/s41567-024-02540-x

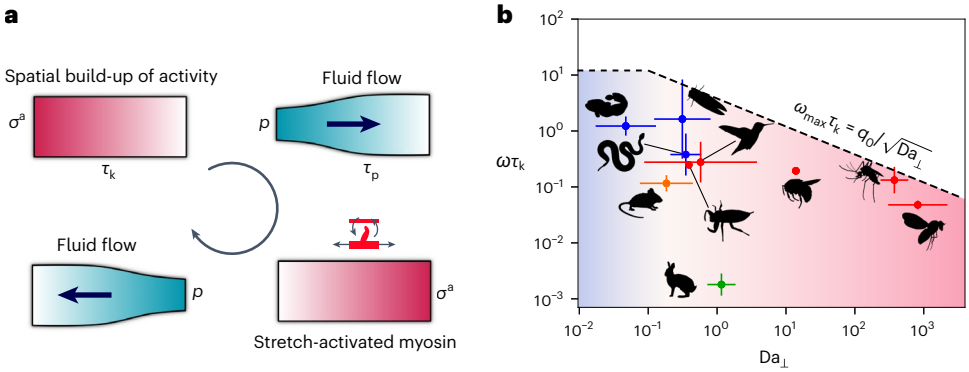

Fig. 3 | Active hydraulics limits muscular contraction rates. a, Active hydraulic oscillations involving a periodic build-up of spatial gradients in active stresses along with fluid flow occur generically with a frequency $\omega \approx 1/\sqrt{\tau_k \tau_p}$ that combines the fast τ_k with the slow τ_p. **b**, Characteristic oscillation frequencies of contractions in fast sonic (blue), flight (red), cardiac (orange) and skeletal (green) muscles across species plotted against the estimated $Da_\perp$ (equation (6)). The data are compiled in Supplementary Table 1 and presented as geometric means with the error bars representing the full range of estimated parameters. Active hydraulic oscillations dominate for $Da_\perp \geq 1$ (red shaded region) with the theoretical scaling limit ω_{max} from equation (7) plotted (dashed line with constant $q_0 \simeq 3.83$ computed for the longest wavelength radial mode; see Supplementary Section VB and Supplementary Fig. 2 for details). When $Da_\perp \ll 1$ (blue shaded region), flow is irrelevant and kinetics dominates, so the oscillation frequency saturates. The data are consistent with our prediction of active hydraulics setting the ultimate limit on muscle contraction rates. Credit: animal silhouettes, Pixabay (cicada and waterbug) and PhyloPic (all others).

$\tau_k = [\omega_{on} + \omega_{off}(y_0)]^{-1}$ (see Supplementary Section II for details) controls the residence time of bound motors and the rate of build-up of active stress. In this situation, if the load-dependent feedback is strong enough ($y_0 \tau_k \omega'_{off}(y_0) > 1$), the molecular reaction develops an oscillatory instability with a characteristic frequency $\omega \approx 1/\tau_k$ (see Supplementary Section III for details). Combining the two limits, and noting that in an anisotropic fibre radial flow dominates axial flow, a key dimensionless parameter emerges—the radial poroelastic Damköhler number:

$$Da_\perp = \frac{\eta}{K_\perp E \tau_k}\left(\frac{R}{\ell_p}\right)^2, \tag{6}$$

which captures the relative importance of radial fluid permeation (a mesoscopic time) in actomyosin kinetics (a molecular time). A similar measure for axial flow can also be constructed (Supplementary Section II). Assuming typical values for $E \approx 0.1$–10 MPa, $\eta \approx 10^{-3}$ Pa s, $\ell_p \approx 20$–60 nm, $\tau_k \approx 1$–10 ms and $R \approx 5$–100 μm (refs. 6,8,39), we obtained a wide range of $Da_\perp \approx 10^{-2}$–10^3 that is accessible to, and seems to be exploited by, the evolutionary range of muscle physiology (Fig. 3b).

When the above effects are all incorporated, an oscillatory instability appears that relies on 'active hydraulics'—that is, a feedback loop coupling poroelastic fluid flow, actives stresses, molecular kinetics and spatial strain gradients (Fig. 3a). Here, a local build-up of active stress (on timescale τ_k) squeezes the sarcomere, forcing fluid to flow and distend neighbouring regions of the lattice (on timescale τ_p), which in turn induces further build-up of myosin via spatial variations in stretch activation. To see this, a minimal one-dimensional (1D) description with $\epsilon_\perp = 0$ suffices (appropriate for *Drosophila* flight muscle[26]). Axial force balance along the muscle fibre implies that $\partial_z[\phi(\sigma^a_{zz} + E\epsilon_{zz}) - (1-\phi)p] = 0$, whereas poroelastic flow dictates that $\partial_t \epsilon_{zz} = K_\parallel(\ell_p^2/\eta)\partial_z^2 p$. Considering the slowest modes on scale of the fibre (L), these equations together (see Supplementary Section IIIA for details) yield $\tau_p \partial_t \epsilon_{zz} \approx -[\epsilon_{zz} + \sigma^a_{zz}/E]$. In the limit where the active stress is bound to the density of bound motors (see Supplementary Section IIIA for details), we can write $\sigma^a_{zz} \approx n_m$ and linearize the kinetics about the steady-state motor density ($n_m = n_m^0 + \delta n_m$, $n_m^0 = \omega_{on}\tau_k$) to obtain $\partial_t \delta n_m = -\delta n_m/\tau_k - \beta\lambda_\parallel n_m^0 \partial_t \epsilon_{zz}$, which includes the feedback mechanism through $\beta = y_0 \omega'_{off}(y_0)/\omega_{off}(y_0) > 0$ (see Supplementary Section IIIA for details). With strong enough activity the coupled dynamics undergoes a Hopf bifurcation, resulting in the spontaneous emergence of active hydraulic oscillations with a characteristic frequency $\omega \approx 2\pi/\sqrt{\tau_k \tau_p}$ that predicts the fruit fly wing-beat frequency $\omega \simeq 150$–160 Hz when using estimates of $\tau_k \approx 0.3$ ms (ref. 4) and $\tau_p \approx 5$–6 s (see Supplementary Section IIIA for details).

For general 3D deformations, fluid is more easily shunted radially (rather than axially) due to a smaller hydraulic resistance across a slender fibre ($R^2/K_\perp \ll L^2/K_\parallel$) and the reduced permeability of Z disks, a feature that survives the inclusion of heterogeneity in pore size. Hence, the radial (that is, fastest) poroelastic time (not the slowest) controls pressure relaxation and is hydraulically rate-limiting. On extending the previous 1D instability calculation to allow for radial flow, spontaneous oscillations emerged with a scaled characteristic frequency (for large $Da_\perp$):

$$\omega\tau_k \propto \frac{1}{\sqrt{Da_\perp}}, \tag{7}$$

that involves both the kinetic and poroelastic timescales; a careful calculation shows that this phenomenon persists more generally (see Supplementary Section III for details). Strikingly, spatiotemporal volumetric deformations trigger active hydraulic oscillations (inevitable for $Da_\perp \geq 1$), even when the instability mechanism is kinetic (see Supplementary Section III for details), hence offering a natural explanation for the experimental data in Fig. 2. Thus we see that active hydraulics, rather than just kinetics, determines the fastest rate of spontaneous muscle contraction; in Fig. 3b we plot the scaling relation in equation (7) and compare it with existing experimental data on muscular contractions across the animal kingdom.

Using representative estimates of the poroelastic, kinetic and contraction timescales in fast sonic (blue), flight (red), cardiac (orange) and skeletal (green) muscles (see Supplementary Section VB and Supplementary Table 1 for details), we found that while synchronous muscles are typically dominated by kinetics ($Da_\perp < 1$, blue shaded region), asynchronous muscles responsible for insect flight are often hydraulically dominated ($Da_\perp \geq 1$, red shaded region), and the data are consistent with the maximal contraction rate being set by active hydraulics. As our analysis focuses on rate limitations intrinsic to muscle fibres, we neglected constraints set by neural and calcium signalling that only affect microscopic kinetics, and can be surpassed in ultrafast contractions (for example, in asynchronous insect flight muscle)[39]. Direct measurements of spatial gradients of deformation and intracellular fluid flow in contracting muscle in the presence and absence of extrinsic control would provide a concrete test of these predictions.

https://doi.org/10.1038/s41567-024-02540-x

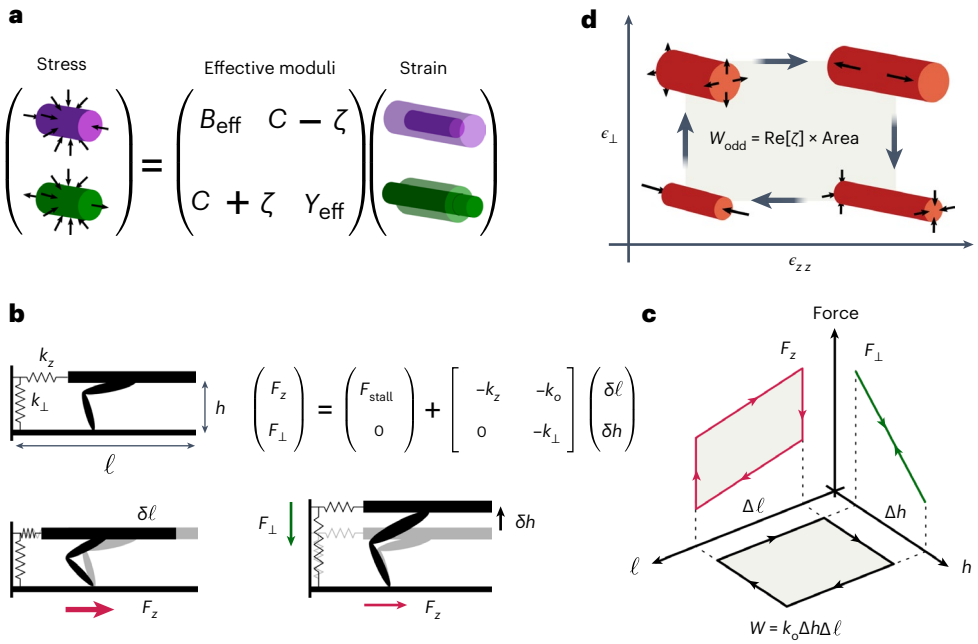

Fig. 4 | Odd elasticity and strain cycle engine in muscle. a, Representation of a stress–strain relation involving shear and volume changes for a 3D continuum material. Muscle fibres are active, so the modulus matrix can be non-symmetric, with the asymmetry quantified by an odd modulus ζ. While the effective bulk (B_{eff}) and Young's (Y_{eff}) moduli are present in isotropic solids, the passive coupling C is only present in anisotropic solids and ζ requires both anisotropy and activity to be present. **b**, The average quasistatic elastic response of a crossbridge is non-reciprocal due to strain-dependent binding kinetics. For $\theta_0 = 0$, axial forces (F_z, magenta arrows) include both active and passive (spring constant k_z) contributions, whereas radial forces ($F_\perp$, green arrows) are purely passive (spring constant $k_\perp$). The linearized force response for small radial and axial stretch about stall shows the non-reciprocal odd spring constant k_o. **c**, The microscopic cycle of axial and radial deformations in a crossbridge generates work proportional to the area of the cycle and the odd spring constant k_o; that is, $W = k_o\Delta h\Delta\ell$. The corresponding axial (F_z) and radial ($F_\perp$) forces are plotted, showing conventional work loops. **d**, Macroscopic odd elasticity (Re[ζ] ≠ 0) produces active work from cycles of axial and radial strains. The work done by the odd modulus (W_{odd}, equation (9)) is proportional to Re[ζ] and the signed area enclosed by the closed loop in strain space.

Non-reciprocal mechanics of an odd elastic engine

Spatial 3D deformations also have unusual mechanical and energetic implications for muscle. The mechanical response of muscle is quantified by a time- or frequency-dependent relation between the total stress (σ_{ij}) and strain (ϵ_{ij}) tensors. For small sinusoidal deformations with frequency ω, a linear response gives $\sigma_{ij}(\omega) = \mathcal{A}_{ijkl}(\omega)\epsilon_{kl}(\omega)$, as shown pictorially in Fig. 4a for shear and isotropic components (see Supplementary Section IV for details). The complex modulus tensor $\mathcal{A}$ includes both an elastic (in-phase) response Re[$\mathcal{A}$] and a viscous (out-of-phase) response Im[$\mathcal{A}$].

In passive systems, time-reversal symmetry enforces $\mathcal{A}_{ijkl}(\omega) = \mathcal{A}_{klij}(\omega)$[40], but in active materials like muscle, energy non-conservation allows non-reciprocal moduli (called odd (visco)elasticity[41] in chiral and active media) that violate a fundamental property of mechanics quantified eponymously as Maxwell–Betti reciprocity[40]. An explicit calculation using our dynamical model (equations (1)–(5)) uncovers the presence of a non-reciprocal odd modulus $\zeta(\omega)$ (Fig. 4a), in addition to activity corrected bulk ($B_{eff}(\omega)$), Young's ($Y_{eff}(\omega)$) and anisotropic ($C(\omega)$) passive moduli; see Supplementary Section IV. In the simplifying limit of horizontal motor binding ($\theta_0 = 0$), the odd modulus is given by:

$$\zeta(\omega) = -\phi N d_m F_{stall}\left(\frac{1-n_m^0}{n_m^0}\right)\frac{|\omega'_{on}(0)|\tau_k}{1+i\omega\tau_k}, \qquad (8)$$

where $F_{stall} = k_m y_0 n_m^0$ is the average stall force and $n_m^0 = \omega_{on}(0)\tau_k$ is the zero-load bound motor fraction (duty-ratio). Equation (8) reveals that, microscopically, odd elasticity originates from the strain-dependent kinetics of a crossbridge (Fig. 4b). As the binding rate depends on the filament spacing (h), a small radial stretch (δh) modifies the active axial force ($F_z = F_{stall} - k_o\delta h$), but an axial stretch ($\delta\ell$) generates no radial force ($F_\perp = 0$). This asymmetric elastic response, quantified by an odd spring constant $k_o \propto F_{stall}|\omega'_{on}(0)|\tau_k \neq 0$, underlies the macroscopic odd modulus ($\zeta \propto -k_o$) and is present in most microscopic crossbridge models (for example, refs. 7,23,29 and references therein). It is worth emphasizing that spatial anisotropy and activity are sufficient for odd (visco) elasticity to emerge in muscle even without chiral effects that are often invoked[42]. Interestingly, the possible presence of such an odd modulus in muscle was noted in passing in old work[43], although its implications were unrecognized.

A unique consequence of non-reciprocal mechanics is the ability to generate work from cycles of strain (Fig. 4c,d). The odd modulus violates energy conservation, so mechanical work becomes history dependent. For a single crossbridge, a quasistatic deformation cycle generates non-zero work $W = -\oint(F_z d\ell + F_\perp dh)$ equal to k_o times the area enclosed by the strain cycle (Fig. 4c). A conventional work loop analysis (that is, area enclosed by the force-displacement curve)[44] recapitulates the same result, provided that all deformations and forces are correctly accounted for (Fig. 4c). For a macroscopic fibre, cyclic contractions at frequency ω generate work $W = -\oint\sigma_{ij}d\epsilon_{ij} = W_{even} + W_{odd}$ ($W > 0$: work produced, $W < 0$: work dissipated) that includes two terms—a strain-rate-dependent viscous term $W_{even} = -\oint dt\,(\mathrm{Im}[\mathcal{A}^e_{ijkl}]/\omega)\dot\epsilon_{ij}\dot\epsilon_{kl}$ and a strain-dependent odd elastic term $W_{odd} = \oint \mathrm{Re}[\mathcal{A}^o_{ijkl}]\epsilon_{kl}d\epsilon_{ij}$ (see Supplementary Section IV for details). The even and odd moduli are $\mathcal{A}^{e,o}_{ijkl} = (\mathcal{A}_{ijkl} \pm \mathcal{A}_{klij})/2$. While W_{even} is simply an anisotropic generalization of standard viscous dissipation ($\mathrm{Im}[\boldsymbol{\mathcal{A}}]/\omega$ is like a viscosity), an intuitive explanation for W_{odd} is that, in the absence of energy conservation, cyclic deformations in different directions do not bring the system back to its initial energy, hence work can be either produced or

https://doi.org/10.1038/s41567-024-02540-x

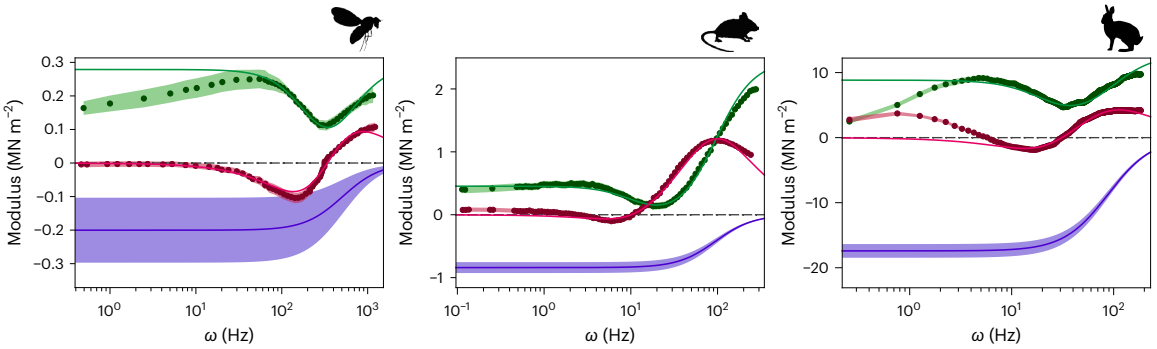

Fig. 5 | Active and non-reciprocal viscoelasticity across muscle types and species. Model fits of linear response (lines) to experimental data (circles are the mean, the shaded regions are 1 s.d.) of sinusoidal uniaxial rheology digitally extracted and compiled from ref. 45 (*Drosophila* flight muscle, left), ref. 46 (mouse cardiac muscle, centre) and ref. 47 (rabbit skeletal muscle, right). As the muscle fibres are small and permeabilized, we assumed affine deformations and neglected pressure gradients (see Supplementary Section VC for fit details). The real and imaginary parts of the response correspond to the elastic (Re[Y_{eff}], green) and the viscous (Im[Y_{eff}], magenta) moduli. Dashed black lines mark zero. The low-frequency response in the experiments sometimes includes a weak power law or logarithmic dependence on frequency, possibly arising from internal passive processes that we neglected. Model estimates using equation (8) of Re[ζ] are shown in blue, with the shaded region denoting 1 s.d. (see Supplementary Section VC for details). Credit: animal silhouettes, PhyloPic.

absorbed. In the axisymmetric limit relevant for muscle, we can simplify W_{odd} as (see Supplementary Section IV for details):

$$W_{\mathrm{odd}} = \frac{\mathrm{Re}[\zeta]}{2}\oint[\epsilon_{zz}\mathrm{d}\epsilon_{\perp} - \epsilon_{\perp}\mathrm{d}\epsilon_{zz}]\,, \qquad (9)$$

that is, work from odd elasticity depends on ζ and the area enclosed by a loop in the space of axial and transverse strains (Fig. 4d). Crucially, this mechanism of power generation relies on 3D spatial deformations (axial and radial), rather than temporal variations.

As a 3D characterization of muscle's viscoelastic response is not yet available, we use our model to analyse experiments[45–47] that measured the 1D uniaxial response (σ_{zz}) of skinned muscle fibres subject to small-amplitude oscillatory axial strains (ϵ_{zz}). Hydraulic effects were assumed to be irrelevant here as the fibres were permeabilized. By compiling data across muscle types and species (*Drosophila* insect flight[45], mouse cardiac[46] and rabbit skeletal[47]), we fit our biophysical model to the measured $Y_{\mathrm{eff}}(\omega) = \sigma_{zz}(\omega)/\epsilon_{zz}(\omega)$ (Fig. 5; see Supplementary Section VC for analysis details).

All three cases show a common behaviour: the elastic modulus (Re[Y_{eff}], green in Fig. 5) has a low-frequency stiffness, a high-frequency rigor response due to crosslinked actomyosin and intermediate softening on timescales when crossbridge cycling allows filaments to slide. The viscous modulus (Im[Y_{eff}], magenta in Fig. 5) is negative at low frequency (hence active and work-producing), switching to positive (dissipative) values at higher frequencies (skeletal muscle displays additional features at low frequency arising from passive dissipation in sarcomeric polymers that we neglected; right panel of Fig. 5). In the 1D setting, the negative viscous modulus offers the only route to produce positive work through temporal changes in strain, and odd elastic effects are absent.

Using our model fit and known structural parameters, we estimated the frequency-dependent Re[ζ] for various muscle types (blue lines in Fig. 5; see Supplementary Section VC for details). Notably, the odd modulus is predominantly negative and it remains non-vanishing at low frequencies (equation (8)). Strain cycles (enclosing negative area) in spontaneous muscle contractions (Fig. 2b,d), have been interpreted as a time-varying Poisson ratio[27], but when combined with our prediction of Re[ζ] < 0 and equation (9), these cycles are predicted to perform active work $W_{\mathrm{odd}} \approx 0.2$–$20$ kPa. Assuming an operation frequency $\omega = 10$ Hz and muscle mass density $\rho_{\mathrm{m}} = 10^3$ kg m^{-3}, we estimated the mass-specific power output $P_{\mathrm{odd}} = \omega W_{\mathrm{odd}}/\rho_m \approx 2$–$200$ W kg^{-1}, which can be significant in physiological conditions[14]. Our predictions of odd elasticity can be directly tested by measuring the 3D structural and force dynamics of muscle fibres using a combination of X-ray-based methods[19,25,28] and force spectroscopy techniques[48].

Discussion

Recognizing the importance of spatial strain gradients and fluid dynamics naturally leads to an emergent maximal rate of muscle contraction ω_{max} based on active hydraulic oscillations that combines molecular, microstructural, macrogeometric and material properties through two timescales, τ_{k} and τ_{p}. Our analysis of published 3D spatial deformation data complements previous temporal studies of muscle rheology and highlights how muscle functions as an active elastic engine, whereby work can be produced from strain cycles via an emergent non-reciprocal response naturally present in anisotropic active solids.

We can estimate the maximal power density P_{max} using a (size-independent) maximal strain ($\varepsilon_{\mathrm{max}}$) and stress ($\sigma_{\mathrm{max}}$) of muscle[49], $P_{\mathrm{max}} \approx \sigma_{\mathrm{max}}\varepsilon_{\mathrm{max}}\omega_{\mathrm{max}}$. When molecular kinetics dominates ($\mathrm{Da}_{\perp} < 1$, $\omega_{\mathrm{max}} \approx 1/\tau_{\mathrm{k}}$), muscular power is not constrained by size ($P_{\mathrm{max}} \propto L^0$). In the active hydraulic regime, however, ($\mathrm{Da}_{\perp} > 1$, $\omega_{\mathrm{max}} \approx 1/\sqrt{\tau_k \tau_p}$), P_{max} decreases with size ($\propto 1/L$), so larger organisms may need additional spring-based mechanisms to amplify power output[50]. Further work incorporating the tissue-scale response, neural control, Ca^{2+} signalling, inertial loading response and so on is required to understand the generality of the phenomena studied here and to connect with more macroscopic approaches to comparative biomechanics[51].

Beyond muscle, the principles of active hydraulics may also apply to other soft contractile systems. For example, most current soft muscle mimetic actuators[52] have contraction rates that are greatly limited by the slow propagation of a diffusive actuation signal, with $\omega_{\mathrm{max}} \approx 1/L^2$ (ref. 53). Our work suggests that if soft actuators were triggered internally, rather than externally, then active hydraulics enables an alternate mechanism for faster contractions with $\omega_{\mathrm{max}} \approx 1/L$. Indeed, this general principle of using local sensing and actuation might be the key to designing faster, stronger and more resilient actuators.

Online content

Any methods, additional references, Nature Portfolio reporting summaries, source data, extended data, supplementary information, acknowledgements, peer review information; details of author contributions and competing interests; and statements of data and code availability are available at https://doi.org/10.1038/s41567-024-02540-x.

References

1. Huxley, A. *Reflections on Muscle* Sherrington Lectures (Liverpool Univ. Press, 1980).

2. Needham, D. M. *Machina Carnis: The Biochemistry of Muscular Contraction in its Historical Development* (Cambridge Univ. Press, 1971).
3. Nyitrai, M. et al. What limits the velocity of fast-skeletal muscle contraction in mammals? *J. Mol. Biol.* **355**, 432–442 (2006).
4. Swank, D. M., Vishnudas, V. K. & Maughan, D. W. An exceptionally fast actomyosin reaction powers insect flight muscle. *Proc. Natl Acad. Sci. USA* **103**, 17543–17547 (2006).
5. Mead, A. F. et al. Fundamental constraints in synchronous muscle limit superfast motor control in vertebrates. *eLife* **6**, e29425 (2017).
6. Gordon, A. M., Homsher, E. & Regnier, M. Regulation of contraction in striated muscle. *Physiol. Rev.* **80**, 853–924 (2000).
7. Powers, J. D., Malingen, S. A., Regnier, M. & Daniel, T. L. The sliding filament theory since Andrew Huxley: multiscale and multidisciplinary muscle research. *Annu. Rev. Biophys.* **50**, 373–400 (2021).
8. Millman, B. M. The filament lattice of striated muscle. *Physiol. Rev.* **78**, 359–391 (1998).
9. Mogilner, A. & Manhart, A. Intracellular fluid mechanics: coupling cytoplasmic flow with active cytoskeletal gel. *Annu. Rev. Fluid Mech.* **50**, 347–370 (2018).
10. Moeendarbary, E. et al. The cytoplasm of living cells behaves as a poroelastic material. *Nat. Mater.* **12**, 253–261 (2013).
11. Skotheim, J. M. & Mahadevan, L. Physical limits and design principles for plant and fungal movements. *Science* **308**, 1308–1310 (2005).
12. Rome, L. C. & Lindstedt, S. L. The quest for speed: muscles built for high-frequency contractions. *Physiology* **13**, 261–268 (1998).
13. Syme, D. A. & Josephson, R. K. How to build fast muscles: synchronous and asynchronous designs. *Integr. Comp. Biol.* **42**, 762–770 (2002).
14. Josephson, R. Contraction dynamics and power output of skeletal muscle. *Annu. Rev. Physiol.* **55**, 527–546 (1993).
15. Szent-Györgyi, A. The contraction of myosin threads. *Stud. Inst. Med. Chem. Univ. Szeged.* **1**, 17–26 (1942).
16. Bugyi, B. & Kellermayer, M. The discovery of actin: "to see what everyone else has seen, and to think what nobody has thought". *J. Muscle Res. Cell Motil.* **41**, 3–9 (2019).
17. Kaminer, B. Water loss during contracture of muscle. *J. Gen. Physiol.* **46**, 131–142 (1962).
18. Trombitás, K., Baatsen, P., Schreuder, J. & Pollack, G. H. Contraction-induced movements of water in single fibres of frog skeletal muscle. *J. Muscle Res. Cell Motil.* **14**, 573–584 (1993).
19. Cecchi, G., Bagni, M., Griffiths, P., Ashley, C. & Maeda, Y. Detection of radial crossbridge force by lattice spacing changes in intact single muscle fibers. *Science* **250**, 1409–1411 (1990).
20. Pinto, J. & Win, R. Non-uniform strain distribution in papillary muscles. *Am. J. Physiol.* **233**, H410–H416 (1977).
21. Neering, I., Quesenberry, L., Morris, V. & Taylor, S. Nonuniform volume changes during muscle contraction. *Biophys. J.* **59**, 926–933 (1991).
22. Ghosh, S. et al. Deformation microscopy for dynamic intracellular and intranuclear mapping of mechanics with high spatiotemporal resolution. *Cell Rep.* **27**, 1607–1620 (2019).
23. Washio, T., Shintani, S. A., Higuchi, H., Sugiura, S. & Hisada, T. Effect of myofibril passive elastic properties on the mechanical communication between motor proteins on adjacent sarcomeres. *Sci. Rep.* **9**, 9355 (2019).
24. Kono, F., Kawai, S., Shimamoto, Y. & Ishiwata, S. Nanoscopic changes in the lattice structure of striated muscle sarcomeres involved in the mechanism of spontaneous oscillatory contraction (SPOC). *Sci. Rep.* **10**, 16372 (2020).
25. Chan, W. P. & Dickinson, M. H. In vivo length oscillations of indirect flight muscles in the fruit fly *Drosophila virilis*. *J. Exp. Biol.* **199**, 2767–2774 (1996).
26. Irving, T. & Maughan, D. In vivo X-ray diffraction of indirect flight muscle from *Drosophila melanogaster*. *Biophys. J.* **78**, 2511–2515 (2000).
27. Cass, J. A. et al. A mechanism for sarcomere breathing: volume change and advective flow within the myofilament lattice. *Biophys. J.* **120**, 4079–4090 (2021).
28. Malingen, S. A. et al. In vivo X-ray diffraction and simultaneous EMG reveal the time course of myofilament lattice dilation and filament stretch. *J. Exp. Biol.* **223**, jeb224188 (2020).
29. Mijailovich, S. M. et al. Three-dimensional stochastic model of actin–myosin binding in the sarcomere lattice. *J. Gen. Physiol.* **148**, 459–488 (2016).
30. Sleboda, D. A. & Roberts, T. J. Internal fluid pressure influences muscle contractile force. *Proc. Natl Acad. Sci. USA* **117**, 1772–1778 (2020).
31. Malingen, S. A., Hood, K., Lauga, E., Hosoi, A. & Daniel, T. L. Fluid flow in the sarcomere. *Arch. Biochem. Biophys.* **706**, 108923 (2021).
32. Wang, H. F. *Theory of Linear Poroelasticity with Applications to Geomechanics and Hydrogeology* (Princeton Univ. Press, 2017).
33. Schoenberg, M. Geometrical factors influencing muscle force development. I. The effect of filament spacing upon axial forces. *Biophys. J.* **30**, 51–67 (1980).
34. Schoenberg, M. Geometrical factors influencing muscle force development. II. Radial forces. *Biophys. J.* **30**, 69–77 (1980).
35. Guo, B. & Guilford, W. H. Mechanics of actomyosin bonds in different nucleotide states are tuned to muscle contraction. *Proc. Natl Acad. Sci. USA* **103**, 9844–9849 (2006).
36. Pringle, J. W. S. The Croonian Lecture, 1977. Stretch activation of muscle: function and mechanism. *Proc. R. Soc. Lond. B* **201**, 107–130 (1978).
37. Ait-Mou, Y. et al. Titin strain contributes to the frank–starling law of the heart by structural rearrangements of both thin-and thick-filament proteins. *Proc. Natl Acad. Sci. USA* **113**, 2306–2311 (2016).
38. Guérin, T., Prost, J. & Joanny, J.-F. Dynamical behavior of molecular motor assemblies in the rigid and crossbridge models. *Eur. Phys. J. E* **34**, 60 (2011).
39. Josephson, R. K., Malamud, J. G. & Stokes, D. R. Asynchronous muscle: a primer. *J. Exp. Biol.* **203**, 2713–2722 (2000).
40. Biot, M. A. *Mechanics of Incremental Deformations* (John Wiley & Sons, 1965).
41. Fruchart, M., Scheibner, C. & Vitelli, V. Odd viscosity and odd elasticity. *Annu. Rev. Condens. Matter Phys.* **14**, 471–510 (2023).
42. Scheibner, C. et al. Odd elasticity. *Nat. Phys.* **16**, 475–480 (2020).
43. Zahalak, G. I. Non-axial muscle stress and stiffness. *J. Theor. Biol.* **182**, 59–84 (1996).
44. Josephson, R. K. Mechanical power output from striated muscle during cyclic contraction. *J. Exp. Biol.* **114**, 493–512 (1985).
45. Tanner, B. C. et al. Thick-to-thin filament surface distance modulates cross-bridge kinetics in drosophila flight muscle. *Biophys. J.* **103**, 1275–1284 (2012).
46. Palmer, B. M. et al. Two-state model of acto-myosin attachment-detachment predicts c-process of sinusoidal analysis. *Biophys. J.* **93**, 760–769 (2007).
47. Kawai, M. & Brandt, P. W. Sinusoidal analysis: a high resolution method for correlating biochemical reactions with physiological processes in activated skeletal muscles of rabbit, frog and crayfish. *J. Muscle Res. Cell Motil.* **1**, 279–303 (1980).
48. Roca-Cusachs, P., Conte, V. & Trepat, X. Quantifying forces in cell biology. *Nat. Cell Biol.* **19**, 742–751 (2017).
49. Marden, J. H. & Allen, L. R. Molecules, muscles, and machines: universal performance characteristics of motors. *Proc. Natl Acad. Sci. USA* **99**, 4161–4166 (2002).

50. Ilton, M. et al. The principles of cascading power limits in small, fast biological and engineered systems. *Science* **360**, eaao1082 (2018).
51. Labonte, D. A theory of physiological similarity in muscle-driven motion. *Proc. Natl Acad. Sci. USA* **120**, e2221217120 (2023).
52. Mirvakili, S. M. & Hunter, I. W. Artificial muscles: mechanisms, applications, and challenges. *Adv. Mater.* **30**, 1704407 (2018).
53. de Gennes, P.-G. A semi-fast artificial muscle. *C. R. Acad. Sci. IIB* **5**, 343–348 (1997).

Methods
The Supplementary Information provides detailed descriptions of the theoretical model, analytical calculations, data acquisition and reanalysis.

Data availability
All original data supporting the findings of this work were obtained from published literature as indicated in Supplementary Section V. Source data are provided with this paper.

Acknowledgements
S.S. acknowledges support from the Harvard Society of Fellows and L.M. acknowledges partial support from the NSF-Simons Center for Mathematical and Statistical Analysis of Biology under grant number 1764269, the Simons Foundation and the Henri Seydoux Fund. We thank S. Srinivasan for useful discussions.

Author contributions
L.M. conceived the research topic and approach. S.S. and L.M. formulated the theoretical model. S.S. performed the analytical calculations, and compiled and analysed the data. S.S. and L.M. wrote the paper.

Competing interests
The authors declare no competing interests.

Additional information
Supplementary information The online version contains supplementary material available at https://doi.org/10.1038/s41567-024-02540-x.

Correspondence and requests for materials should be addressed to Suraj Shankar or L. Mahadevan.

Peer review information *Nature Physics* thanks Kenneth Campbell, and the other, anonymous, reviewer for their contribution to the peer review of this work.